Astron. Astrophys. 362, 371–378 (2000)

ASTRONOMY AND ASTROPHYSICS

Characteristics of quiet Sun cell and network brightenings

L.K. Harra[1], **P.T. Gallagher**[2], **and K.J.H. Phillips**[3]

[1] Mullard Space Science Laboratory, University College London, Holmbury St. Mary, Dorking, Surrey RH5 6NT, UK
[2] Big Bear Solar Observatory, New Jersey Institute of Technology, 40386 North Shore Lane, Big Bear City, CA 92314–9672, USA
[3] Department of Space Science and Technology, Rutherford Appleton Laboratory, Chilton, DIDCOT, Oxon OX11 0QX, UK

Received 10 April 2000 / Accepted 16 August 2000

Abstract. Extreme ultraviolet observations of the quiet Sun are made with the Coronal Diagnostic Spectrometer (CDS) on board the Solar and Heliospheric Observatory (SOHO). It has been previously noted that frequent transition region brightenings occur in both the bright network and dark cell regions. Analysing 1125 events, we determined the characteristics of the brightenings in the cell and network regions which include the duration, energy, and intensity increase above the background. Network brightenings are found to be larger than cell events occurring with a mean duration of 150 s and releasing an average of $10^{26.9}$ ergs per event. Cell brightenings, on the other hand, last for an average of 96 s and release $10^{25.8}$ ergs per event. It has also been found that the distribution of energy is a power-law which is different in the cell (γ=2.5) and network (γ=1.5) regions. When the entire quiet Sun region is analysed the value of γ is 1.7. The number of events per CDS pixel is approximately the same, and a histogram of the ratio ([peak value – background]/background) shows similar values for both the cell and network. It is important to analyse the cell and network regions separately in the context of coronal heating by such small flare-like events.

Key words: Sun: corona – Sun: transition region – Sun: UV radiation

1. Introduction

There has been much discussion in recent years about the fast and frequent brightenings which occur in the quiet Sun. These events have been observed since *Skylab* (e.g. Vernazza et al., 1975). Since the launch of both SOHO and *Yohkoh* higher resolution has been obtained which is yielding new information on these brightenings and their contribution to coronal heating. Krucker et al. (1997) discovered temporal variations in the soft X-ray emission from *Yohkoh* Soft X-ray telescope (SXT) and radio emission from the VLA at quiet Sun network locations. Extrapolations over the whole Sun imply one brightening every three seconds. The events reported here are an order of magnitude smaller than previously measured bright points or transient active region brightenings. Further study by Benz & Krucker (2000) using SOHO EIT (EUV Imaging Telescope) and VLA data have revealed that chromospheric emission (He II) peaks before the coronal emission (Fe IX/X and Fe XII). They draw an analogy between this time lag and the lag observed in regular flares between the hard X-ray impulsive burst and the main phase soft X-ray burst. The close temporal correlation between transition region emission (in particular O V enhancements) with hard X-ray emission has been well documented (e.g. Woodgate et al. 1983). They therefore concluded that the coronal brightenings observed in the quiet Sun are likely to be caused by the same process that causes regular flares.

Harrison (1997) detected EUV brightenings at network junctions which he called 'blinkers' using the coronal diagnostic spectrometer (CDS) on board SOHO. He found that different temperature plasmas displayed a different level of variation, and that the blinkers activity is confined to transition region and chromospheric temperatures. The blinker events in this study contain about 10^{-6} the thermal energy of a large flare, i.e. their thermal energy is approximately 10^{26} ergs, and hence can be considered as microflares. Most of this work has concentrated on the larger network brightenings. This work was extended by Harrison et al. (1999) who analysed 97 blinkers in detail. They found that O V, O IV and O III blinkers have average enhancements of 1.48, 1.43 and 1.28 respectively while the Mg IX and Mg X blinkers have lower enhancements. They emphasize the importance of these blinker events which occur in the transition region for the heating of the solar corona.

There have been many theories put forward to explain how the corona is heated. These include acoustic waves, magnetohydrodynamic (MHD) waves, and magnetic reconnection (e.g. Ulmschneider et al., 1991). It has been found that acoustic waves do not possess enough energy to heat the corona unless they have high frequencies (e.g. Moe & Nicolas, 1997, Bruner, 1978). There is a similar problem with dissipating the energy of high frequency MHD waves. This is discussed by Oughton et al. (1999) where they introduce an indirect method of damping low frequency Alfven waves. In this method a proportion of the Alfven waves are reflected and interact with the upward propagating Alfven waves to produce quasi 2D MHD turbulence, which dissipate the energy in small scales. This was modelled for coronal hole heating. A statistical description of MHD turbulence has been carried out by Einaudi & Velli (1999). They have shown that MHD turbulence gives similar behaviour to

Send offprint requests to: L.K. Harra (lkh@mssl.ucl.ac.uk)

the power-law histograms of energy release. Sturrock (1999) has investigated the consequences of reconnection occurring at chromospheric levels rather than in the corona, finding that chromospheric reconnection can lead to Joule heating of coronal gas. These results emphasize the importance of understanding the lower solar atmosphere in order to understand coronal heating.

As mentioned, one of the theories for coronal heating is that many small reconnection events ('nanoflares', i.e. events with energies of $\approx 10^{23}$ ergs) are responsible for heating the corona (Levine 1974, Parker 1981, 1983, 1988). The energy distribution of these small flare-like events appears to be a power-law following the form $f(E) = f_o E^{-\gamma}$. Microflares or nanoflares can explain the heating of the corona only if $\gamma > 2$ (Hudson, 1991). Wheatland (2000) has investigated the distribution of flares for individual active regions. He concludes that the flare power-law size distribution reflects an intrinsic property of the flare mechanism, and is independent of physical parameters within active regions.There have been a number of recent investigations into the energy distribution in the quiet Sun using the instruments on board the SOHO and Transition Region and Coronal Explorer (TRACE spacecraft). Coronal iron images (Fe IX/X, Fe XII) from SOHO EIT have been studied by Krucker & Benz (1998). It was found that the frequency distribution of microflares is approximately power-law with γ ranging between 2.3 and 2.6, marginally larger than that required for nanoflare heating. This result was confirmed by the high-resolution TRACE images in both the 195 and 173 Å wavelength bands analysed by Parnell & Jupp (2000). They found that the power-law determined is dependent on the line-of-sight depth chosen. For a constant line-of-sight depth, γ was found to lie between 2.4 and 2.6, whereas for a line-of-sight depth proportional to the $area^{1/2}$ γ is lower, lying between 2.0 and 2.1. However, Berghmans et al. (1998) used EIT images in the coronal Fe lines and chromospheric He II line to look at the characteristics of the transition region and corona. Power-law distributions were found for the histograms of the radiative losses both in He and the Fe lines with γ=1.9$\pm$0.1 for the former and γ=1.35$\pm$0.2 for the latter. The brightenings in the corona and chromosphere are clearly different. There is, in summary, some dispute over the actual values of the power-law, with coronal values ranging from γ=1.35 $\rightarrow$ 2.6.

Recent work has tended to concentrate on network brightenings which are associated with magnetic bipolar regions which disappear after approximately one day (Schrijver et al., 1998). Bipolar fields have been observed in the cell regions, and these are estimated to provide approximately 10% of the more intense network concentrations, drifting towards the network by supergranular convection (Zhang et al., 1998). High-resolution magnetograms from the Big Bear Solar Observatory (BBSO) have been used to investigate the evolution of the cell magnetic fragments (Zhang et al., 1998). They found that the cell magnetic elements emerge everywhere within the supergranular cell with no preferred location. They also found that 22% of the total magnetic flux in quiet regions was in the form of cell magnetic flux. Using high-resolution SOHO Michelson Doppler Imager (MDI) magnetograms and EUV images from CDS, O'Shea et al. (2000) show that bright network regions, such as network junctions, overlie 11% of the total quiet Sun magnetic flux, while the remaining network overlies 59% and the cell only 30%.

It seems then that there are significant brightenings in the cell interior related to the small magnetic fragments found in the cells. A study of the quiet Sun using EIT (Berghmans et al., 1999) illustrates this well, when they showed that 100% of the transition region shows variability - both in the dark cell interiors and network regions. Wikstol et al. (2000) have analysed spectral time series data from SUMER specifically in the internetwork regions. They find small amplitude Doppler shift oscillations both at chromospheric and transition region temperatures. The intensity variations associated with these are small, and are suggested to be due to acoustic waves. Gallagher et al. (1999) have investigated the velocities in the transition region and the chromosphere. They find that the transient events are observed in both cell and network regions, with those in the cell regions being smaller and of shorter duration. Redshift velocities were found in both the cell and network regions with the cell velocities being lower. The differing properties of the cell and network were attributed to different heating mechanisms. For the cell region they favour acoustic waves forming shocks, whereas for the network regions nanoflare like magnetic reconnection events dominate.

It is clear that the characteristics of the cell and network brightenings need to be investigated separately. It is well established that there are more brightenings in the transition region than in the corona (e.g. Brkovic et al., 2000) and that there are intensity fluctuations both in the cell and network regions (e.g. Berghmans et al., 1998). It is important to understand the transition region brightenings and their relationship to coronal emission in order to understand coronal heating. In this paper we concentrate on the O V transition region emission, and investigate properties of the cell and network regions. In particular we concentrate on the duration, emission measure, energy and energy power-law distributions. In the next section, the SOHO CDS observing sequence used is described. In Sect. 3, the techniques used to extract the brightenings are defined. Sect. 4 gives a description of the methods we used to separate the cell and network regions. Sect. 5 gives the results and Sect. 6 discusses the implications of the observations.

2. Observations

The SOHO Coronal Diagnostic Spectrometer (CDS) (Harrison et al., 1995) consists of the Normal Incidence Spectrometer (NIS) and the Grazing Incidence Spectrometer (GIS) covering the wavelength range 150–800 Å covering lines formed in the temperature range T_e=10^4 - 10^6 K.

Observations were carried out on 1996 December 19 using the NIS predefined studies NTBRMDI1 and NTBRMDI2. The purpose of these studies is to look for fast brightenings in the quiet Sun. First, in the NTBRMDI1 study the NIS makes a 240 $\times$ 240 arcsec context image in O V (629 Å) and He I (584 Å). Secondly, in the NTBRMDI2 the NIS 4 $\times$ 240 arcsecs slit,

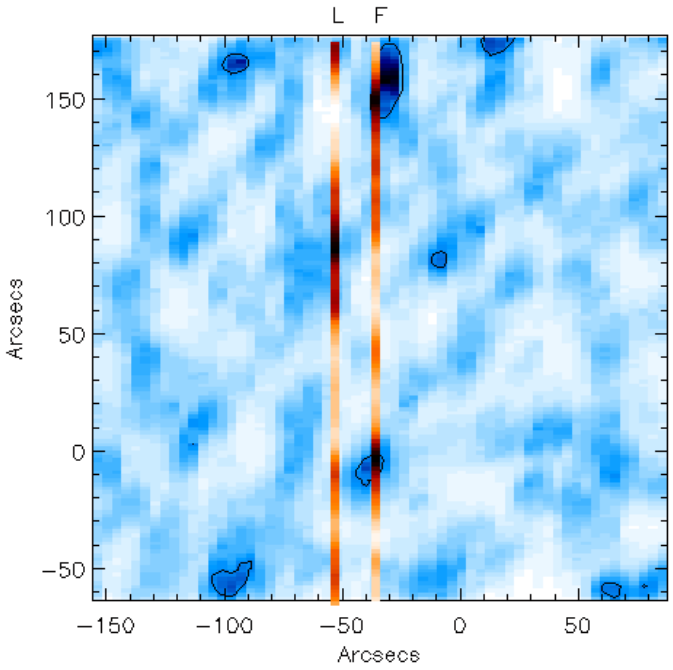

Fig. 1. An example of the CDS study NTBRMDI1 taken on the 19 Dec 1996 in O V. The first and last slit positions are shown as F and L respectively. The fast slit study NTBRMDI2 ran between 13:24 UT and 15:16 UT

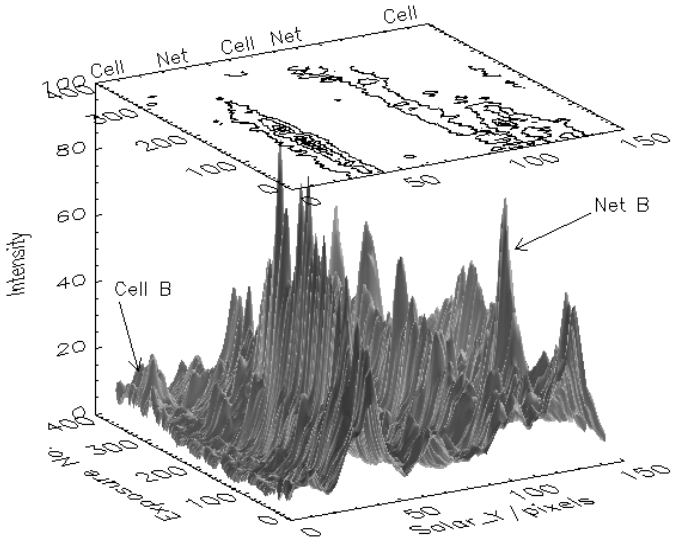

Fig. 2. A surface plot of O V intensity which clearly illustrates the weak brightenings occurring in cell regions as well as in the network regions. One cell and one network brightening are marked as "Cell B" and "Net B" respectively. The contours in the plot above the surface plot outline the brighter network structures (but do not show individual brightenings), and the cell and network regions are labelled. The space axis (in pixels: 1CDS pixel=4arcsecs^2) is aligned along the CDS slit (south→ north is 0→150); the time axis is equivalent to a West-to-East space dimension, generated as the CDS slit moves from position F in Fig. 1 to position L at a rate of 9 arcseconds per hour.

orientated N–S, is set at the same location for two hours. Both O V and He I were observed with an exposure time of 15s. A total of 360 exposures were made during 1hr 53 mins. The study was not in 'Solar Feature Tracking' mode, and hence during the observations the features observed move across the slit by solar rotation. This motion is at the slow rate of 9 arcseconds per hour. Further details of these observing sequences are given in Gallagher et al. (1999). The observation is shown in Fig. 1 where we have the O V context image, with the first and last slit positions marked. In the following we will discuss only the O V data since the brightenings are much more readily apparent than in He I and the network is not as well defined. This is possibly due to resonance scattering as discussed in Gallagher et al. (1999) and Macpherson & Jordan (1997). Another alternative is discussed in Patsourakos et al. (1999). They suggest that it is not the opcaity causing the different appearance in He I, but that it can be explained by its sensitivity to coronal radiation.

As discussed in Harrison (1997), UV brightenings are detected at the network junctions, i.e. where two or more supergranular cells meet. In the present study we found that brightenings occur both in the network and in the cell regions. The brightenings in the cell regions can be seen in Fig. 2, which shows a surface plot of the intensity along the slit with time.

3. Data analysis

The standard CDS software was used to remove cosmic rays, correct for the CCD readout bias and flatfielding, and intensity calibrated to convert the raw data to absolute units (photons/cm^2/s/arcsec^2). The O V spectral line (629 Å) was extracted at each spatial pixel and fitted with a Gaussian profile in order to determine the intensity. The emission measure at each spatial location was then determined by assuming the temperature is the peak of the emissivity or $G(T)$ function.

It is necessary to define the brightenings both in the spatial and temporal direction. This is discussed in the following two subsections.

3.1. *Defining the brightenings temporally*

Firstly the local points of minima were determined. A minimum was defined as a point which had three points on either side with values of emission measure greater than it. Next the background was removed. This is illustrated in Fig. 3 and Fig. 4 for the network and cell respectively. The brightenings are smaller in size and the background is lower in the cell.

The peaks were then defined as those points which *have* one point on one side and two points on the other side lower than it and in addition to have flux at least 10% above the background level. We found a total of 1125 brightenings during our observing period of two hours satisfying these criteria. The time profiles of these brightenings were then fitted using a spline fit, and the total intensity, peak intensity and duration of each brightening were determined. A surface plot of these brightenings, with time and distance axes and with the background removed is shown in Fig. 5. The peaks are uniformly spread across the region of quiet Sun with no obvious preference given to the network regions.

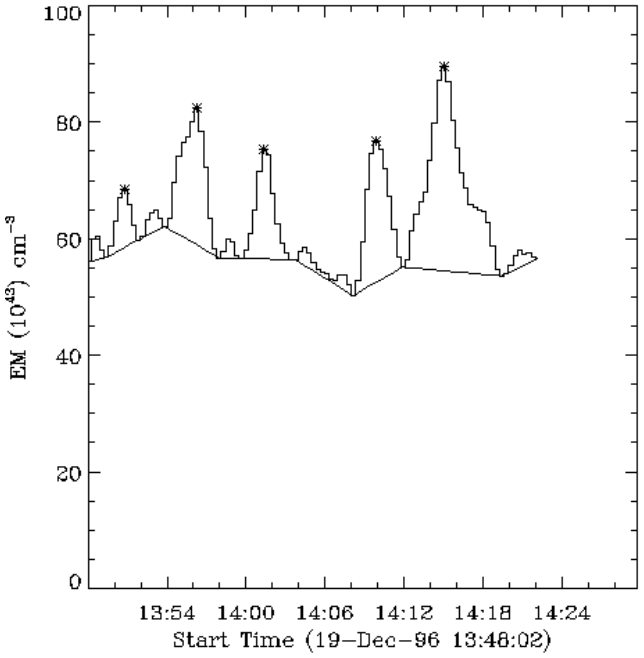

Fig. 3. Example of the O V brightenings measured in the network. The asterisks show the defined brightenings. The solid line shows the derived background.

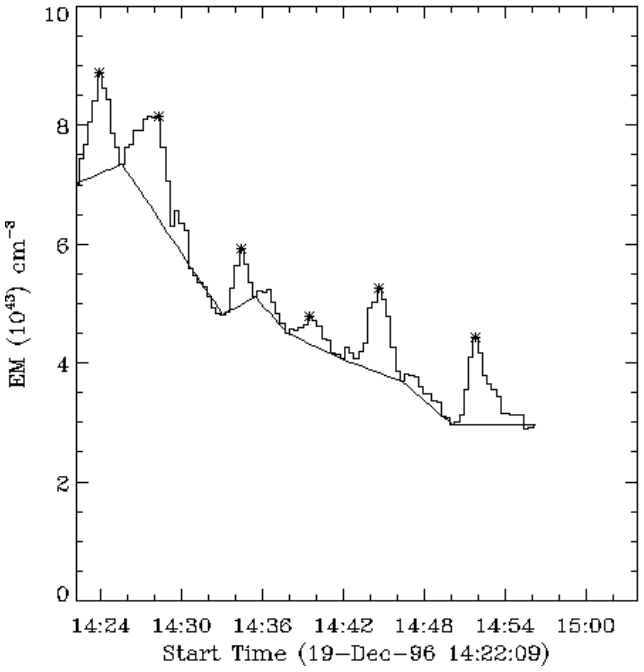

Fig. 4. Example of the O V brightenings measured in the cell. The asterisks show the defined brightenings and the solid line shows the derived background.

3.2. Defining the brightenings spatially

The next problem is that of "event splitting" described in Shimizu (1997) and Krucker & Benz (1998) in the context of small X-ray brightenings. Each individual brightening may occur over several pixels and hence be measured several times. To account for this we used a process called "blob-colouring". If a spatial pixel contains a peak, then the pixels surrounding it are searched to see if peaks occur within a time period of 15 secs. If any are found then these are considered to be one peak only. The emission measure value of the peak pixel is taken to be the maximum value.

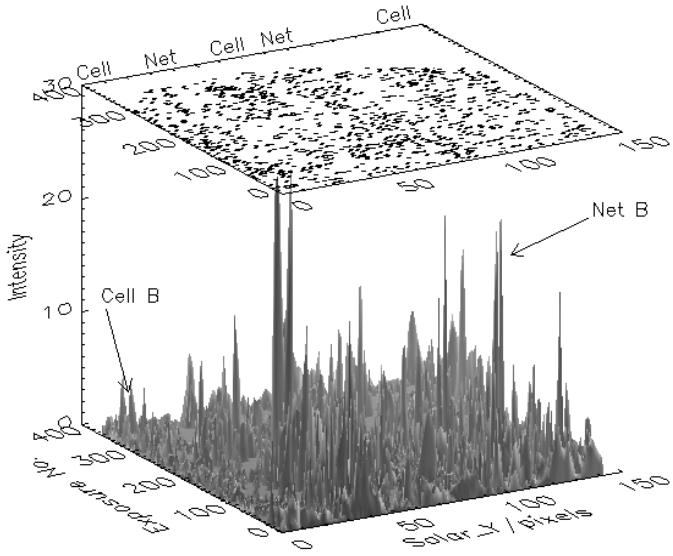

Fig. 5. A surface plot showing the background removed O V intensity. The locations of the defined peaks are indicated as dots on the figure above the surface plot. There are many brightenings which occur nearly uniformly throughout the quiet Sun regardless of the presence of network or cell.

4. Separating the cell and network regions: image thresholding

Previous work has separated the cell and network region by fitting two Gaussians to the dataset (e.g. Reeves et al., 1976). For this work it is crucial to separate the cell and network regions as accurately as possible. To do this we separated the cell and network regions of the space–time image using the optimal thresholding technique which is based on locating the minimum in the image's intensity histogram (Gonzalez & Wintz, 1987, Gupta & Sortrakul, 1998, Chow & Kaneko, 1972) and improves on previous work published by Gallagher et al. (1998). In order to model the brightness distribution of the image, we suppose that the image is composed of only two principal brightness regions representing the cell and the network. The intensity histogram can then be expressed as

$$F(I) = \frac{P_c}{\sqrt{2\pi}\sigma_c}\exp\left\{-\frac{(I-\mu_c)^2}{2\sigma_c^2}\right\} + \frac{P_n}{\sqrt{2\pi}\sigma_n}\exp\left\{-\frac{(I-\mu_n)^2}{2\sigma_n^2}\right\} \quad (1)$$

where μ_c and μ_n are the mean values of the cell and network distributions, σ_c and σ_n are the standard deviations and P_c and P_n are the component weights such that

$$P_c + P_n = 1. \quad (2)$$

As the mean intensity of the cell region is lower than that of the network regions, we may define a threshold level T so that all the pixels with an intensity below T are considered to belong to the cell, while all pixels with levels above T belong to the network. The threshold is defined as the intensity level at which

$$\frac{P_c}{\sqrt{2\pi}\sigma_c}\exp\left\{-\frac{(T-\mu_c)^2}{2\sigma_c^2}\right\} = \frac{P_n}{\sqrt{2\pi}\sigma_n}\exp\left\{-\frac{(T-\mu_n)^2}{2\sigma_n^2}\right\} \quad (3)$$

which can be rearranged and simplified to produce the quadratic equation

$$AT^2 + BT + C = 0 \quad (4)$$

where

$$\begin{aligned} A &= \sigma_c^2 - \sigma_n^2 \\ B &= 2(\mu_c\sigma_n^2 - \mu_n\sigma_c^2) \\ C &= \sigma_c^2\mu_n^2 - \sigma_n^2\mu_c^2 + 2\sigma_c\sigma_n ln(\sigma_n P_c/\sigma_c P_n) \end{aligned} \quad (5)$$

The intensity histogram was then fitted with two Gaussians and the optimal threshold evaluated by solving Eq. 4. The upper panel of Fig. 6 shows the cell and network Gaussian fits to the O V histogram together with the optimal threshold for the data, while the lower panel shows the corresponding space–time image overlayed with contours drawn at the optimal threshold intensity level.

Each pixel was then classified as belonging to the cell or the network distributions using the following rules;

$$(x,y) = \begin{cases} \text{cell} & \text{if } I(x,y) < T \\ \text{network} & \text{if } I(x,y) > T \end{cases} \quad (6)$$

An important step before applying the above methodology involves increasing the local minimum between the cell and network brightness distributions. There are several techniques by which this can be achieved (see Weszka & Rosenfield, 1979) but in this case smoothing the data using a boxcar filter was found to be the most effective. The smoothing operation simply reduces small scale brightness variations across the image and produces two semi–continuous regions.

5. Results

Of the 1125 brightenings, 733 were in the cell regions and 392 in the network region. In the 1hr and 53 mins observation, there were 0.019 brightenings/CDS pixel (1 CDS pixel = 4 arcsecs) for the network regions and 0.023/CDS pixel for the cell regions. The network events are more intense by approximately a factor of 10.

The purpose of the analysis is to investigate the differences between the brightenings which occur in the cell and those in the network. The emission measure distribution is shown in Fig. 7. As expected the emission measure values in the cell are lower than those in the network.

The total thermal energy derived from the O V emission line ($E = 3nkTV$, where n is the density, k is Boltzman's constant, T is the temperature and V is the volume) was derived from the emission measure by assuming a volume. The area was determined from the "blob colouring" technique mentioned earlier, and the volume was assumed to be area$^{3/2}$. Fig. 8 shows the energy distribution. There is a peak in the cell energy and the total region energy of approximately $10^{25.8}$ ergs. More probably, the number of brightenings in reality falls monotonically from small energy values ($< 10^{25.8}$ ergs), but the observed distribution shows this peak because the CDS sensitivity is limited to those events with energies greater than about $10^{25.5}$ ergs.

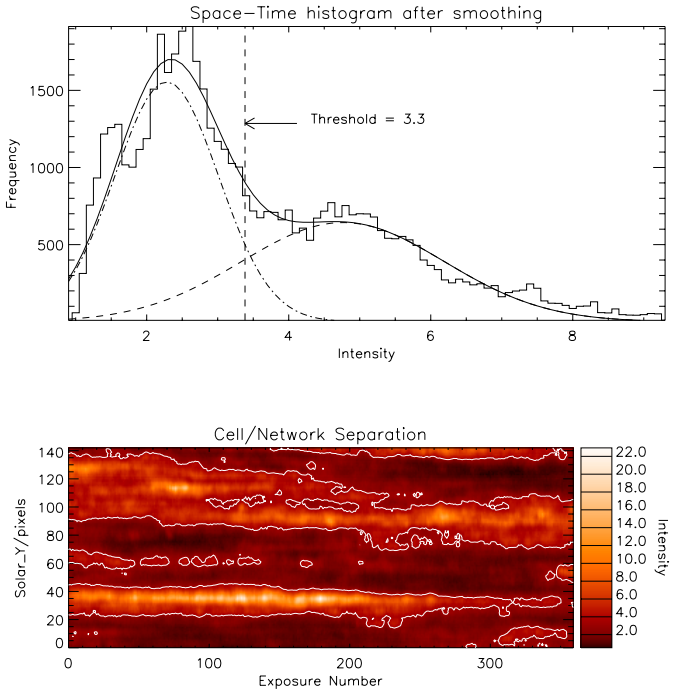

Fig. 6. (Upper panel) The intensity histogram of the O V smoothed space–time image together with the two Gaussians representing the cell and network populations. (Lower panel) The corresponding space–time image overlayed with contours at the optimal threshold.

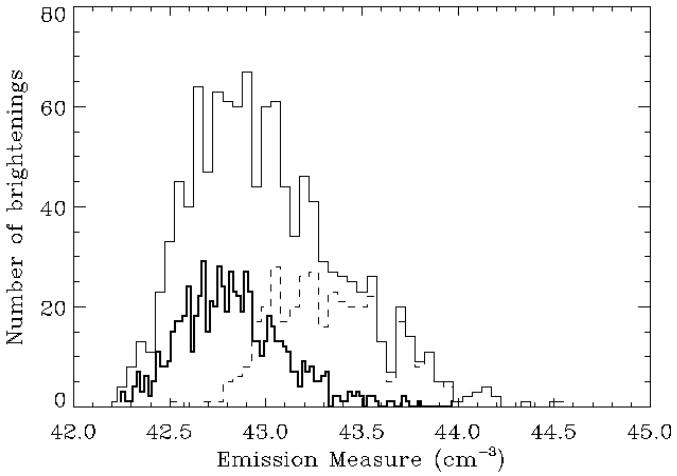

Fig. 7. The solid line shows the total emission measure, the thick line shows the cell emission measure and the dashed line shows the network emission measure.

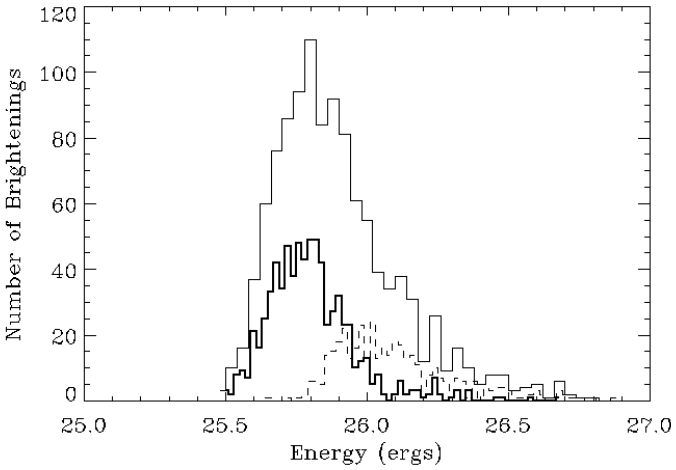

Fig. 8. The solid line shows the total energy, the thick line shows the cell energy and the dashed line shows the network energy.

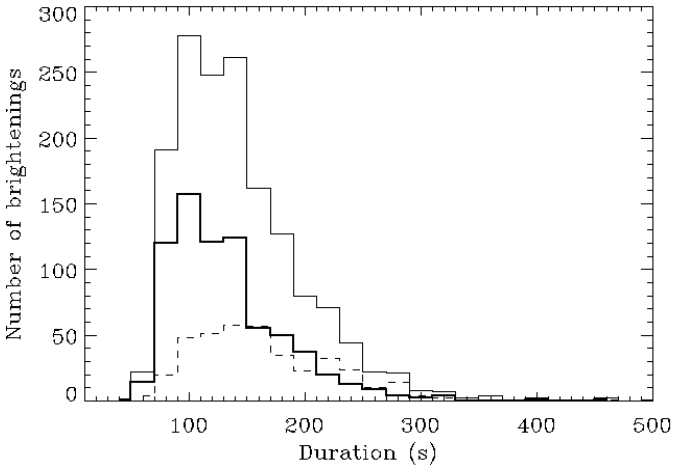

Fig. 10. The solid line shows the total duration, the thick line shows the cell duration and the dashed line shows the network duration.

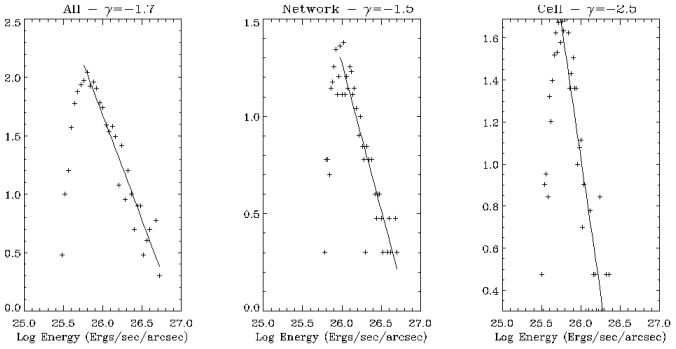

Fig. 9. Log (frequency of brightening) vs log (energy), shown as a solid line for the whole quiet Sun region (left), the network region only (middle) and the cell region only (right).

Hence there is most likely many much smaller events that were not detected in this analysis.

Parnell & Jupp (2000) demonstrated the dependence of the value of the power-law index (γ) on the line-of-sight depth chosen. To determine the power-laws for the cell, network and the total region, we chose a line-of-sight depth equal to the $\sqrt{(area)}$. We make the same assumptions for all three cases, and hence can easily compare our results.

The best fit power-law to the decreasing part of the energy distribution (see Fig. 9) was determined by least squares. The peak occurred at approximately $10^{25.8}$ ergs, and we took that value as the minimum in the fit. The rising part of the energy distribution most likely arises by selection effects, and hence events with smaller energies are not all observed. The χ^2 values derived for the total region is 0.59, for the network region is 0.87 and for the cell region is 3.45. Different power-laws were derived when we considered the whole area, and the network and the cell regions separately. The cell region has the highest power-law index, γ, indicating that there are many more smaller brightenings occurring.

The distribution of durations of the brightenings is shown in Fig. 10. The network brightenings last longer than the cell brightenings. These events have a shorter duration than the larger blinkers observed by Harrison et al. (1999) who observed longer duration blinkers which increased the average duration of their events to be 2400 s. The durations we observe are on average 100s. The sizes of our brightenings range from 1 CDS pixel to 5 CDS pixels (1.68 arcsecs to 8.4 arcsecs). Only 4% of the cell brightenings are greater than 1 CDS pixel in size, whereas 17% of the network brightenings are greater than 1 CDS pixel in size.

The ratio of the peak value (background subtracted) to the background was determined and this is illustrated in Fig. 11. The background is determined by the method described in Sect. 3 and shown in Figs. 3 and 4. We assumed that the peak had at least one lower value on one side and at least two lower values on the other, and that it was at least 10% above the background level. Interestingly most of the events in both the cell and network regions are equal to a value of 10% above the background.

Table 1 summarises the characteristics of the cell, network and quiet Sun region. The average values for the duration, Log EM, Log energy and the ratio of (peak–background) to background were determined by fitting a spline to the histograms, and determining the peak value and the errors are determined from the value at half-maximum. The errors for γ are determined from the standard deviations from the first degree polynomial fit to the data. As can be seen, there is a large difference in the results if we observe the cell and network regions separately or if we look at the whole quiet Sun region. This has an impact on our understanding of the heating mechanism(s) which take place.

6. Discussion and conclusions

Recently there has been a lot of work carried out on the dynamics in the quiet Sun - specifically in order to determine the heating mechanism. Two main types of activity in the quiet Sun are blinkers and explosive events. The latter were discovered by the NRL HRTS experiment (e.g. Dere et al. 1989). They are high-velocity events which it has been suggested are caused

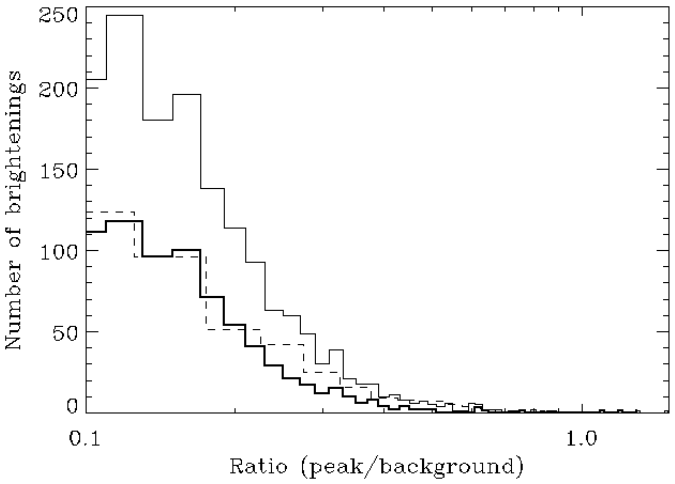

Fig. 11. The solid line shows the Ratio (peak–background)/background for the total quiet Sun region, the thick line shows the cell Ratio (peak–background)/background and the dashed line shows the network Ratio (peak–background)/background.

Table 1. Mean properties of the cell, network and quiet Sun events.

	Network	Cell	Total quiet Sun
Duration (s)	$150\ ^{+64}_{-64}$	$96\ ^{+56}_{-24}$	$100\ ^{+70}_{-28}$
Log EM (cm^{-3})	$43.2\ ^{+0.5}_{0.3}$	$42.7\ ^{+0.4}_{-0.1}$	$42.9\ ^{+0.3}_{-0.4}$
Log Energy (ergs)	$26.9\ ^{+0.0}_{-0.01}$	$25.8\ ^{+0.1}_{-0.16}$	$25.8\ ^{+0.2}_{-0.2}$
γ	1.5 ± 0.1	2.7 ± 0.2	1.5 ± 0.2
No. of events/CDS pixel	0.019	0.023	0.020
Peak/Background	$0.1\ ^{+0.08}_{-0.0}$	$0.11\ ^{+0.06}_{-0.01}$	$0.11\ ^{+0.06}_{-0.01}$

by small-scale reconnection events. The relationship between blinkers and explosive events was investigated by Chae et al. (2000). They discovered that blinkers consist of many small-scale, short-lived brightening events as observed by SUMER. It is suggested that all these different events are produced by the same physical mechanism - magnetic reconnection. It has also been noted that brightenings exist in both the bright network and dark cell regions (e.g. Brkovic et al. 1999, Gallagher et al., 1999, Berghmans et al. 1998). The purpose of this work is to investigate the network and cell brightenings and determine their similarities and differences.

We found that the main difference between the cell and network brightenings is the fact that the network brightenings have energies an order of magnitude larger than the cell brightenings. The durations of the network events are longer than the cell events. The power-law distribution of energy shows that the value of γ for the cell is higher than in the network. This indicates that the cell region is dominated by smaller brightenings.

The cell and network regions are similar in that the ratio of (peak–background)/background is the same at 0.1. In our definition we had assumed that any peak has to be 10% above the background. This suggests that there are many more smaller brightenings which are harder to define and that the more sensitive an instrument we use the more brightenings we will see. The occurence of brightenings in cell and network regions per unit area is approximately the same.

It has been strongly suggested that photospherically generated acoustic waves which turn into shocks in the chromosphere are responsible for the heating of the cell regions in the chromosphere. This was discovered through a relationship between velocities and intensities of low ionization stages (Carlsson et al. 1997). This effect is not easily seen in the transition region, although there is some indication of a 3-minute period through a preliminary wavelet analysis by Gallagher et al. (1999). The heating mechanism in the transition region is still in dispute

There are many similarities in the events in the cell and network regions which is indicative that they are formed by the same mechanism except on a different scale. The work by Zhang et al. (1998) shows that 22% of the magnetic field in the quiet Sun is in the cell regions, and that it emerges all through the region and not just at the centre as previously thought. This suggests that there is every possibility that magnetic reconnection is also taking place in the cell regions. Further work will be carried out using MDI and TRACE to study these smaller events to search for a relationship between bipolar regions and brightenings.

Acknowledgements. LKH is grateful to PPARC for the award of an Advanced Fellowship. SOHO is a mission of international cooperation between ESA and NASA. The authors are grateful to Dr. J-C. Vial for helping improve the clarity of the paper.

References

Benz A.O., Krucker S., 1999, A&A 341, 286
Berghmans D., Clette F., Moses D., 1998, A&A 336, 1039
Brkovic A., Ruedi I., Solanki S.K., et al., 2000, A&A 353, 1083
Brokvic A., Ruedi I., Solanki S.K., 1999, Proceedings of the 8th SOHO workshop, ESA SP-466
Bruner E., 1978, ApJ 226, 1140
Carlsson M., Judge P.G., Wilhelm K., 1997, ApJ 486, L63
Chae J., Wang H., Goode P., Fludra A., Schuhle U., 2000, ApJ 528, L119
Chow C.K., Kaneko T., 1972, Computers and Biomedical Research 5, 388
Dere K.P., Bartoe J.-D.F., Brueckner G.E., 1989, Solar Phys. 123, 41
Einaudi G., Velli M., 1999, Physics of Plasmas Vol. 16, No. 11, 4146
Gallagher P.T., Phillips K.J.H., Harra-Murnion L.K., Baudin F., Keenan F.P., 1999, A&A 348, 251
Gallagher P.T., Phillips K.J.H., Harra–Murnion L.K., Keenan F.P., 1998, A&A 335, 733
Gonzalez R., Wintz P., 1987, Digital Image Processing. 2nd ed., Addison–Wesley
Gupta L., Sortrakul T., 1998, Pattern Recognition 31, 315
Harrison R.A., Sawyer E.C., Carter M.K., et al., 1995, Solar Phys. 162, 233
Harrison R.A., 1997, Solar Phys. 175, 476
Harrison R.A., Lang J., Brooks D.H., Innes D.E., 1999, A&A 351, 1115
Hudson H.S., 1991, Solar Phys. 133, 357
Krucker S., Benz A.O., Bastian T.S., Acton L.A, 1997, ApJ 488, 499
Krucker S., Benz A.O., 1998, ApJ 501, L213
Krucker S., Benz A.O., 2000, Solar Phys. 191, 341

Levine R.H., 1974, ApJ 190, 447
Macpherson K.P., Jordan C., 1997, The Corona and Solar Wind near Minimum Activity. ESA SP-404, 533; Trans. R.S. A 281, 319
Moe O., Nicolas K.R., 1977, ApJ 211, 579
O'Shea E., Gallagher P.T., Mathioudakis M., Phillips K.J.H., Keenan F.P., 2000, A&A in press
Oughton S., Matthaeus W.H., Zank G.P., Mullan D.J., 1999, ESA SP-466, 525
Parker E.N., 1981, ApJ 244, 644
Parker E.N., 1983, ApJ 264, 642
Parker E.N., 1988, ApJ 330, 474
Parnell C.E., Jupp P.E., 2000, ApJ 529, 554
Patsourakos S., Vial J.-C., Gabriel A.H., Bellamine N., 1999, ApJ 522, 540
Reeves E.M., Vernazza J.E., Withbroe G.L., 1976, Phil.
Schrijver C.J., Title A.M., Harvey K.L., et al., 1998, Nat 394, 152
Shimizu T., 1997, Ph.D. Thesis, University of Tokyo
Sturrock P., 1999, ApJ 521, 451
Ulmschneider P., Priest E.R., Rosner R., 1991, Mechanisms of Chromospheric and Coronal Heating. Springer, Berlin
Vernazza J.E., Foukal P.V., Noyes R.W., et al., 1975, ApJ 199, L123
Weszka J.S., Rosenfeld A., 1979, IEEE Transactions on Systems, Man, and Cybernetics 9, 38
Wheatland M.S., 2000, ApJ 532, 1209
Wikstol O., Hansteen V.H., Carlsson M., Judge P.G., 2000, ApJ 531, 1150
Woodgate B.E., Shine R.A., Poland A.I., Orwig L.E., 1983, ApJ 265, 530
Zhang J., Lin G., Wang H., Zirin H., 1998, A&A 338, 322